Dual transformation for wave packet dynamics: Application to Coulomb systems

doi: 10.1063/1.480281

Dual transformation for wave packet dynamics: Application to Coulomb systems

Isao Kawata and Hirohiko Kono[a)]
Department of Chemistry, Graduate School of Science, Tohoku University, Sendai 980-8578, Japan

(Received 4 May 1999; accepted 9 September 1999)

A dual transformation technique that can deal with awkward Coulomb potentials is developed for electronic wave packet dynamics. The technique consists of the variable transformation of the Hamiltonian and the transformation of the wave function with a normalization constraint. The time evolution is carried out by the alternating-direction implicit method. The operation of the transformed Hamiltonian on the wave function is implemented by using three- and five-point finite difference formulas. We apply it to the H atom and a realistic three-dimensional (3D) model of H_2^+. The cylindrical coordinates ρ and z are transformed as $\rho=f(\xi)$ and $z=g(\zeta)$, where ξ and ζ are scaled cylindrical coordinates. Efficient time evolution schemes are provided by imposing the variable transformations on the following requirements: The transformed wave function is zero and analytic at the nuclei; the equal spacings in the scaled coordinates correspond to grid spacings in the cylindrical coordinates that are small near the nuclei (to cope with relatively high momentum components near the nuclei) and are large at larger distances thereafter. No modifications of the Coulomb potentials are introduced. We propose the form $f(\xi)=\xi[\xi^n/(\xi^n+\alpha^n)]^\nu$. The parameter α designates the ρ-range where the Coulomb potentials are steep. The $n=1$ and $\nu=\frac{1}{2}$ transformation provides most accurate results when the grid spacing $\Delta\xi$ is sufficiently small or the number of grid points, N_ξ, is large enough. For small N_ξ, the $n=\frac{1}{2}$ and $\nu=1$ transformation is superior to the $n=1$ and $\nu=\frac{1}{2}$ one. The two transformations are also applied to the dissociation dynamics in the 3D model of H_2^+. For the $n=\frac{1}{2}$ and $\nu=1$ transformation, the main features of the dynamics are well simulated even with moderate numbers of grid points. The validity of the two transformations is also enforced by the fact that the missing volume in phase space decreases with decreasing $\Delta\xi$. © *1999 American Institute of Physics.* [S0021-9606(99)30145-8]

I. INTRODUCTION

Femtosecond technology has opened up a new field of study as to coherent electronic motions such as electron transfer between nuclei in molecules.[1–3] The intensity can be so high to induce tunneling ionization. In the high-intensity and low-frequency range, the Coulomb potential distorted by the laser electric field forms a ''quasi-static'' barrier through which an electron can tunnel.[4–9] Special attention has been paid to new nonlinear optical processes such as above-threshold ionization[10–12] and high-order harmonic generation of emission.[13–19] High-order harmonics are generated when the ejected electron circles back to the vicinity of the nucleus (rescattering).[9] Electronic dynamics in intense fields involves such large amplitude motions like rescattering. For molecules, nuclear motion is also involved in the dynamics of the system. Recent experiments and theories in a strong laser field case ($>10^{11}\,\mathrm{W/cm^2}$) have underscored the combined process of photodissociation and photoionization. It has been experimentally revealed that the kinetic energies of fragments are consistent with Coulomb explosions at specific internuclear distances in the range of 7–10 a.u.[20–24] An explanation for this finding is as follows: Ionization rates at the critical internuclear distances exceed those near the equilibrium internuclear distance and those of dissociative fragments, and ionization to higher charge states occurs when the nuclei pass through the critical range.[25–29] The fact that ionization is enhanced at critical internuclear distances suggests that strong correlation between the electronic motion and the nuclear configuration/motion exists in intense laser fields.

Although various numerical methods for electronic dynamics in laser fields have been proposed,[30–39] it is not an easy task to simulate, e.g., large amplitude motions of an electronic wave packet. It is even harder to include the quantum-mechanical motion of nuclei. There exist two approaches to simulate electronic dynamics in intense fields. One is the expansion using spatially delocalized bases. In this approach, the time-dependent wave function is expanded in terms of state-specific states, i.e., bound, autoionizing, and scattering states of the field-free Hamiltonian.[37–39] The time-dependent Schrödinger equation describing the interaction with a laser pulse is transformed into a system of coupled first-order differential equations for time-dependent coefficients. This technique has been successfully applied to atoms (not applied to molecules yet), although the number of coupled equations usually exceeds tens of thousands. For the motion of a spatially localized wave packet induced by an intense laser pulse, however, the delocalization of state-specific states leads to poor convergence.

The grid representation is complementary to the state-

a)Electronic mail: kono@mcl.chem.tohoku.ac.jp

specific expansion approach.[32–36] Conventional time evolution methods using grid representations,[40,41] such as split operator techniques combined with fast Fourier transform,[42,43] have been successfully applied to the nuclear wave packet dynamics in molecular physics. The success is attributed to the nonsingularity that internuclear (adiabatic/diabatic) potentials are usually expressed in terms of analytic functions of internuclear distances. On the other hand, for electronic dynamics, one must cope with the awkward Coulomb potential characterized by its long range and its singularity at the origin (at the nucleus for electron–nucleus interaction). The grid boundary in coordinate space must be chosen to be far from the origin to accommodate the wave function and grid spacings must be small to reproduce high momentum components generated near the origin. Because of those difficulties, the performance of the conventional grid methods is very poor for Coulomb systems.

Recently, we have been developing an efficient grid method to simulate electronic dynamics accurately.[44] The choice of coordinate systems is crucial. In Ref. 44, the following three requirements are imposed on the coordinate system to be employed: (i) The wave function is transformed so that it is zero at the Coulomb singular point (which ensures that the numerical difficulties concerning the singularity are avoided); (ii) the differential operators can be well evaluated by the finite difference method even near the Coulomb singular points; (iii) the equal spacings in the new (scaled) coordinates correspond to grid spacings in the cylindrical coordinates that are small near the nuclei (to cope with relatively high momentum components near the nuclei) and are large at larger distances therefrom. The transformed Schrödinger equation is discretized in space with the help of finite difference formulas, and is integrated in time by the alternating-direction implicit method (ADI).[45–47] Among various propagation methods, the ADI method is found to be the most accurate for steep attractive potentials, at least for the one-dimensional Coulomb potential. We have applied the method to H.[44] The cylindrical coordinate ρ for the electron is transformed as $\rho=\xi^{3/2}$, where ξ is a scaled coordinate. This transformation satisfies the above three requirements and drastically reduces the required number of grid points.

We have also succeeded in including nuclear motion for a realistic 3D model of H_2^+.[1,2] Although the nuclear motion is restricted to the polarization direction z of the laser electric field (perpendicular to ρ), the electron moves in three-dimensional space. The two electronic coordinates z and ρ and the internuclear distance R are treated quantum mechanically without using the Born–Oppenheimer approximation. We have investigated effects of the nuclear motion on enhanced ionization and on electron transfer between the two nuclei. Correlations between the electronic and nuclear motions are extracted from the full dynamical calculation.

In this paper, we generalize the ''dual transformation'' technique, i.e., the method of consistently transforming both of the wave function and the Hamiltonian for wave packet dynamics. The transformation of ρ is expressed as $\rho=f(\xi)$, where the function is chosen to satisfy the three requirements (i)–(iii) described above. Scaling is extended to the unscaled z coordinate as $z=g(\zeta)$. Various functions of the transformations are examined in different ranges of grid spacings $\Delta\xi$ and $\Delta\xi$, by comparing the wave packet calculated by the dual transformation technique with the exact one. Another method for determining the transformation efficiency is the classical phase space analysis[48] based on the fact that wave packets decay exponentially in classically forbidden regions of phase space. To that end, the transformed Hamiltonian is divided into a kinetic energy and a potential; then, the classical phase space covered by the grid representation is estimated.

The rest of this paper is organized as follows. The general framework of dual transformation is given in Sec. II. In Sec. III, some bench mark tests are carried out for H and the 3D model of H_2^+. Various transformations are tested; the wave packets computed by our method are compared with the exact ones. The phase space analysis is also used to enforce the validity of efficient transformations. Finally, in Sec. IV, concluding remarks are given with a brief summary of the present work.

II. METHODOLOGY

A. Dual transformation

In this work, we apply the dual transformation technique to H and the 3D model of H_2^+ employed in Ref. 35. In the model, the following assumptions are made: The electric field of the applied laser is linearly polarized along the z axis; the nuclear motion is restricted to the polarization direction. Because of the cylindrical symmetry, the z component of the electronic angular momentum, $m\hbar$, is conserved; the electronic degrees of freedom to be considered are two cylindrical coordinates z and ρ.

The center-of-mass motion of this three-body system can be separated from internal coordinates such as ρ and z. Here, ρ and z are measured with respect to the center of mass of the two nuclei.[49] The Hamiltonian for the internal motions is written as (throughout this paper atomic units are used)

$$H=-\frac{1}{m_p}\frac{\partial^2}{\partial R^2}-\frac{1}{2\mu}\left(\frac{\partial^2}{\partial\rho^2}+\frac{1}{\rho}\frac{\partial}{\partial\rho}+\frac{\partial^2}{\partial z^2}\right)+\frac{m^2}{2\rho^2}+\frac{1}{R}+V(\rho,z,R)+V_{\mathcal{E}}(z,t), \tag{2.1}$$

where R is the internuclear distance, m_e and m_p are electron and nuclear masses, and

$$\mu=\frac{2m_pm_e}{2m_p+m_e}. \tag{2.2}$$

The potential $V(\rho,z,R)$ is the sum of the Coulomb interactions

$$V(\rho,z,R)=-\frac{1}{\sqrt{\rho^2+(z-R/2)^2}}-\frac{1}{\sqrt{\rho^2+(z+R/2)^2}}, \tag{2.3}$$

and $V_{\mathcal{E}}(z,t)$ is the dipole interaction between the molecule and the electric field $\mathcal{E}(t)$ of a laser pulse

$$V_{\mathcal{E}}(z,t)=z\mathcal{E}(t). \tag{2.4}$$

If the finite masses of protons are taken into account, $z\mathcal{E}(t)$ should be multiplied by $1+m_e/(2m_p+m_e)$. For the H atom, the R-degree of freedom is eliminated from Eq. (2.1), and Eq. (2.3) is replaced with $-1/\sqrt{\rho^2+z^2}$ (μ is the reduced mass of H).

We would like to spatially discretize the Hamiltonian to solve the time-dependent Schrödinger equation

$$i\frac{\partial}{\partial t}\phi(\rho,z,R)=H\phi(\rho,z,R). \tag{2.5}$$

The finite difference method is chosen to evaluate the differential operators contained in the Hamiltonian. It should, however, be noted that the Coulomb potential is characterized by its singularity at the nucleus and its long range. For the cylindrical coordinate system, the finite difference method does not give sufficient accuracy. We propose here the generalized cylindrical coordinate system as

$$\rho=f(\xi),\quad z=g(\zeta), \tag{2.6}$$

where f and g are functions of scaled coordinates ξ and ζ [$f(\xi)=\xi$ and $g(\zeta)=\zeta$ lead to ordinary cylindrical coordinates]. It has been known that in electronic structure calculations variable transformations (scaling, mapping procedures) efficiently reduce the number of representation points.[48,50–56] Variable transformation has been also introduced to calculate electronic wave packet dynamics.[32]

In addition to the variable transformation of the Hamiltonian, we have to transform the wave function to avoid the numerical difficulties concerning the Coulomb singularity. The original wave function $\phi(f(\xi),g(\zeta),R)$ which is in general finite at the nuclei must be transformed to a function $\psi(\xi,\zeta,R)$ that is zero at the nuclei. This demand on the transformed wave function, i.e., the requirement (i) in Sec. I, must be satisfied under a normalization condition. The original wave function $\phi(\rho,z,R)$ is normalized as

$$\int_0^\infty dR\int_0^\infty d\rho\int_{-\infty}^\infty dz\rho|\phi(\rho,z,R)|^2=1. \tag{2.7}$$

When the finite difference method is used, it is generally difficult to conserve the norm of the wave function. It has been known[44] that to make stable and accurate the time evolution scheme, based on the finite difference method, the following normalization condition should be imposed on the transformed wave function $\psi(\xi,\zeta,R)$

$$\int_0^\infty dR\int_0^\infty d\xi\int_{-\infty}^\infty d\zeta|\psi(\xi,\zeta,R)|^2=1. \tag{2.8}$$

Note that the volume element for normalization is $dR\,d\xi\,d\zeta$ not like $\xi\,dR\,d\xi\,d\zeta$.

The transformed wave function that satisfies the normalization condition Eq. (2.8) is uniquely determined as

$$\psi(\xi,\zeta,R)=\sqrt{f(\xi)f'(\xi)g'(\zeta)}\,\phi(f(\xi),g(\zeta),R), \tag{2.9}$$

where a function with a prime denotes the derivative with respect to its argument. Inserting Eq. (2.9) into Eq. (2.5), one obtains the following Schrödinger equation:

$$i\frac{\partial\psi(\xi,\zeta,R)}{\partial t}=\hat{H}\psi(\xi,\zeta,R), \tag{2.10}$$

where the transformed Hamiltonian $\hat{H}$ is given by

$$\hat{H}=K_R+K_\xi+K_\zeta+\frac{m^2}{2\rho^2}+V+V_{\mathcal{E}}. \tag{2.11}$$

The kinetic-energy parts with respect to coordinates ξ, ζ, and, R, i.e., K_ξ, K_ζ, and K_R are expressed as

$$K_\xi=T_\xi+\frac{1}{4\mu f'^4(\xi)}\left[\frac{7}{2}f''^2(\xi)-f'(\xi)f'''(\xi)\right]-\frac{1}{8\mu f^2(\xi)}, \tag{2.12a}$$

$$K_\zeta=T_\zeta+\frac{1}{4\mu g'^4(\zeta)}\left[\frac{7}{2}g''^2(\zeta)-g'(\zeta)g'''(\zeta)\right], \tag{2.12b}$$

$$K_R=-\frac{1}{m_p}\frac{\partial^2}{\partial R^2}, \tag{2.12c}$$

where

$$T_\xi=-\frac{1}{4\mu}\left[\frac{1}{f'^2(\xi)}\frac{\partial^2}{\partial\xi^2}+\frac{\partial^2}{\partial\xi^2}\frac{1}{f'^2(\xi)}\right], \tag{2.13a}$$

$$T_\zeta=-\frac{1}{4\mu}\left[\frac{1}{g'^2(\zeta)}\frac{\partial^2}{\partial\zeta^2}+\frac{\partial^2}{\partial\zeta^2}\frac{1}{g'^2(\zeta)}\right]. \tag{2.13b}$$

The dual transformation is named after the two transformations, i.e., the variable transformation of the Hamiltonian and the transformation of the wave function with the normalization constraint Eq. (2.8).

B. Time evolution with the alternating-direction implicit method

The formal solution of Eq. (2.10) is expressed as

$$\psi(t_{n+1})=\hat{T}\exp\left[-i\int_{t_n}^{t_{n+1}}\hat{H}(t')dt'\right]\psi(t_n)$$
$$=\exp[-i\Delta t\hat{H}(t_{n+1/2})]\psi(t_n)+O(\Delta t^3), \tag{2.14}$$

where $\psi(t_n)$ is the wave function at time $t_n=n\Delta t+t_0$ and $\hat{T}$ is the time ordering operator. The Hamiltonian in the second version of Eq. (2.14) is that at the midpoint of the time step, $t_{n+1/2}=t_n+\Delta t/2$. If the time step Δt is sufficiently small, the propagator $\exp[-i\Delta t\hat{H}(t_{n+1/2})]$ can be replaced with an approximate propagator that is accurate up to a certain order of Δt. The wave function at the desired time is obtained by operating such a short time propagator on the wave function iteratively.

It has been known that the alternating-direction implicit method (ADI) provides short time propagators of which quality is characterized by the second-order accuracy in time and the stability for various potentials. In addition to these points, as will be demonstrated, the ADI is amenable to variable transformations. The ADI embodies the powerful idea of operator splitting and time splitting. In the following, we briefly review a 3D version of the ADI. Let us assume that $\hat{H}(t_{n+1/2})$ is decomposed into three operators $A(t_{n+1/2})$, $B(t_{n+1/2})$, and $C(t_{n+1/2})$. According to the ADI, the time evolution operator $\exp[-i(A+B+C)\Delta t]$ is expressed as

$$e^{-i(A+B+C)\Delta t}=\frac{1}{1+iA\Delta t/2}\frac{1}{1+iB\Delta t/2}\frac{1-iC\Delta t/2}{1+iC\Delta t/2}\times(1-iB\Delta t/2)(1-iA\Delta t/2)+O(\Delta t^3). \tag{2.15}$$

The actual operation on the wave function is separated into three steps by introducing ''artificial'' intermediate states $\psi^{n+1/3}$ and $\psi^{n+2/3}$

$$(1+iC\Delta t/2)\psi^{n+1/3}=(1-iC\Delta t/2)(1-iB\Delta t/2)\times(1-iA\Delta t/2)\psi(t_n), \tag{2.16a}$$

$$(1+iB\Delta t/2)\psi^{n+2/3}=\psi^{n+1/3}, \tag{2.16b}$$

$$(1+iA\Delta t/2)\psi(t_{n+1})=\psi^{n+2/3}, \tag{2.16c}$$

which is known as the D'yakonov scheme.[46] The wave function $\psi(t_{n+1})$ can be obtained by solving Eqs. (2.16a)–(2.16c) in order. As shown below, the dynamics of the electronic and nuclear wave packet can be pursued without invoking any approximations such as the Born–Oppenheimer separation of electronic and nuclear degrees of freedom.

When the differential operators involved in *A*, *B*, and *C* are chosen to be those of different degrees of freedom, Eq. (2.16) can be reduced to three sets of one-dimensional implicit problems such as the Cranck–Nicholson scheme.[45,46] For H_2^+, the three operators K_ζ, K_ξ, and K_R in the Hamiltonian Eq. (2.11) must be confined in *A*, *B*, and *C* separately. We furthermore divided the Coulomb interactions into nucleus–nucleus interaction $1/R$ and electron–nucleus interaction $V(\rho,z,R)$. The most reasonable way of separation is as follows:

$$A=K_\zeta+\tfrac{1}{2}V(\rho,z,R)+V_{\mathcal{E}}(z,t_{n+1/2}), \tag{2.17a}$$

$$B=K_\xi+\frac{1}{2}V(\rho,z,R)+\frac{m^2}{2\rho^2}, \tag{2.17b}$$

$$C=K_R+\frac{1}{R}. \tag{2.17c}$$

In the above equations, V is divided into halves so that $A\psi$ and $B\psi$ vanish at the nuclei. This ensures that not only $\psi(t_n)$ but also intermediates $\psi^{n+1/3}$ and $\psi^{n+2/3}$ are zero at the nuclei.

We apply the finite difference method to evaluate the differential operators. For instance, Eq. (2.16a) is then reduced to a set of systems of simultaneous linear algebraic equations for the unknown $\psi^{n+1/3}$: Equations (2.16a)–(2.16c) can be reduced to three sets of systems of simultaneous equations. The systems of equations are tridiagonal for the three-point finite difference scheme and pentadiagonal for the five-point finite difference scheme. Suppose that the numbers of grid points for ξ, ζ, and R are N_ξ, N_ζ, and N_R, respectively. For Eq. (2.16a), we obtain $N_\zeta N_\xi$ band diagonal systems of simultaneous equations; each band diagonal system has N_R unknowns. The band diagonal systems of equations can be solved efficiently by using *LU* decomposition.

C. Explicit forms for variable transformation

We are now in a position to explicitly determine f and g functions of scaled coordinates ξ and ζ. To fulfill the three requirements (i)–(iii) in Sec. I, we choose the following forms:

$$f(\xi)=\xi\left(\frac{\xi^n}{\xi^n+\alpha^n}\right)^\nu, \tag{2.18a}$$

$$g(\zeta)=[1-(1-\beta)\exp(-\zeta^2/\gamma^2)]\zeta, \tag{2.18b}$$

where the parameters α and γ are widths of ρ- and z-ranges where the potential V is relatively deep, and β is the parameter to shorten ζ-grid spacings near $z=0$. Around the singular points (located along $\xi=0$), the prefactor $\sqrt{ff'g'}$ changes as $\approx\sqrt{(1+n\nu)\beta}\,\xi^{(2n\nu+1)/2}/\alpha^{n\nu}$. The requirement (ii) that the transformed wave function must be analytic, demands that the order of the power of ξ, $(2n\nu+1)/2$, must be a natural number. The number $n\nu$ must be chosen out of half odd numbers. Then, the transformed wave function given by Eq. (2.9) is zero at the nuclei; the requirement (i) is automatically fulfilled.

Inverting equally spaced points in ξ and ζ onto ρ and z, one finds that the grid spacings in ρ and z are proportional to f' and g', respectively. As ξ increases, f' changes from $(1+n\nu)(\xi/\alpha)^{n\nu}$ to 1; as ζ increases, g' changes from β to 1. When $\beta<1$ and $\alpha\gg\Delta\xi$, the requirement (iii) is met. Then, grid spacings along ρ- and z-directions decrease as approaching to the singular points. When the cylindrical coordinate system ($\alpha=0$ and $\beta=1$) is employed, the split operator time evolution technique together with the use of FFT (fast Fourier transform) is applicable to the transformed Hamiltonian (because the prefactors of the differentials in the transformed Hamiltonian are independent of the coordinates), but the efficiency as a numerical method is very low. Poor performance of the cylindrical coordinate system originates from the fact that the requirements (ii) and (iii) are not satisfied. For the cylindrical coordinate system, the transformed wave function is not analytic around the nuclei because $\sqrt{ff'g'}\approx\sqrt{\rho}$. The Fourier series expansion of the transformed wave function converges very slowly.

In Eq. (2.13a), the symmetrized product form of $\partial^2/\partial\xi^2$ and $1/f'^2(\xi)$ is adopted as well as in Eq. (2.13b). If symmetric difference formulas are applicable to T_ξ, the grid representation of the symmetrized product form is symmetric: The grid representation of K_ξ is then still Hermitian. The norm is, hence, strictly conserved (without numerical roundoff errors). However, the grid representation of

$$\frac{\partial^2}{\partial\xi^2}\frac{\psi(\zeta,\xi,R)}{f'^2(\xi)},$$

at the point $\xi=\Delta\xi$ next to the line $\xi=0$ requires evaluating $\psi(\xi,\zeta,R)/f'^2(\xi)\propto\xi^{(1-2n\nu)/2}$ at $\xi=0$, which is generally nonzero. It is not allowed to simply put the boundary condition $\psi(\xi=0,\zeta,R)=0$ into the element. To avoid this difficulty in the actual numerical scheme, we use an asymmetric form

$$K_\xi = -\frac{1}{2\mu f'^2(\xi)}\left[\frac{\partial^2}{\partial\xi^2} - \frac{2f''(\xi)}{f'(\xi)}\frac{\partial}{\partial\xi}\right] - \frac{1}{4\mu f'^4(\xi)}\left[\frac{5}{2}f''^2(\xi) - f'(\xi)f'''(\xi)\right] - \frac{1}{8\mu f^2(\xi)}. \tag{2.19}$$

This form is still Hermitian, but the finite difference representation is only approximately symmetric except when f is a linear function of ξ (cylindrical coordinate ρ). We will show that the loss of population due to the asymmetry is negligible when the transformation functions f and g are chosen properly. The quality of this representation will be discussed in Sec. III.

Here the differential operators in Eqs. (2.19) and (2.12b) are evaluated using three- or five-point finite difference formulas. Accordingly, appropriate boundary conditions must be imposed on the transformed wave function $\psi(\xi,\zeta,R)$. At the grid end points $\xi_{\max}$, $\zeta_{\max}$, $R_{\min}$ and $R_{\max}$, $\psi(\xi_{\max},\zeta,R) = \psi(\xi,\pm\zeta_{\max},R) = \psi(\xi,\zeta,R_{\min}) = \psi(\xi,\zeta,R_{\max}) = 0; \psi(\xi=0,\zeta,R) = 0$ (from the nature of the transformed wave function).

Chelkowski *et al.*[35] have solved Eq. (2.5) with the help of the Bessel–Fourier expansion in the ρ variable. This allows one to eliminate the singularities in the Laplacian and in the potential and to use a split operator propagation method together with FFT in z and R. In the dual transformation approach, the transformed Schrödinger Eq. (2.10) is solved by employing the ADI method.

III. RESULTS AND DISCUSSION

A. Application to H

We first apply our method to the time evolution of a hydrogen atom in the case where no laser field is turned on and the atom is initially (at $t=0$) in the ground state $1s$. We designate the field-free transformed Hamiltonian as $\hat{H}_0$. It should be pointed out that the time evolution of $1s$ is the worst case in applying the present method. As the average of the radial coordinate becomes larger, the steep fall of the Coulomb potential around the nucleus damages the accuracy less severely. Since only two variables ξ and ζ are involved, we use the Peaceman–Rachford method[57,58] which is a two-dimensional version of the ADI method. The time evolution for Δt is then separated into two steps: $(1+iB\Delta t/2)\psi^{n+1/2} = (1-iA\Delta t/2)\psi(t_n)$ and $(1+iA\Delta t/2)\psi(t_{n+1}) = (1-iB\Delta t/2)\psi^{n+1/2}$.

We demonstrate how much the norm and overlap of the $1s$ state calculated by our method decrease or change with time. The norm and overlap are defined as $\langle\psi^f_{1s}(t)|\psi^f_{1s}(t)\rangle$ and $\langle\psi^f_{1s}(0)|\psi^f_{1s}(t)\rangle$, respectively, where $\psi^f_{1s}(0)$ is the discretized wave function whose amplitudes at the grid points are identical with the analytic $1s$ transformed wave function $\psi_{1s} = \sqrt{2f(\xi)f'(\xi)g'(\zeta)}\exp(-\sqrt{f^2(\xi)+g^2(\zeta)})$, and $\psi^f_{1s}(t)$ denotes the time evolution of $\psi^f_{1s}(0)$ for the *discretized* form of the field-free transformed Hamiltonian, $\hat{H}'_0$. The integrals with respect to ξ and ζ are performed by using the trapezoidal rule.

It should be noted that $\psi^f_{1s}(0)$ is not identical with the ground state of the *discretized* Hamiltonian $\hat{H}'_0$, ψ'_{1s}. The initial wave function $\psi^f_{1s}(0)$ includes excited-state components $\{\psi'_{2s},\psi'_{3s},\ldots\}$ of $\hat{H}'_0$, i.e., $\psi^f_{1s}(0) = \Sigma c_j(0)\psi'_j$, where j runs from $1s$ (c_{1s} is dominant). As the discretized form is better approximated to the Hamiltonian (2.11), the norm and overlap at $t=0$ are closer to unity and the difference between ψ'_{1s} and $\psi^f_{1s}(0)$ becomes smaller ($c_{1s}\sim 1$).

The time evolution of ψ^f_{1s} calculated by our method is expressed as

$$\psi^f_{1s}(t) = \sum_j c_j(t)\psi'_j \exp(-itE'_j), \tag{3.1}$$

where E'_j are eigenvalues of $\hat{H}'_0$ and $c_j(t)$ are expected to be slowly varying functions of time. The norm and overlap change with time as $\langle\psi^f_{1s}(t)|\psi^f_{1s}(t)\rangle = \Sigma|c_j(t)|^2$ and $\langle\psi^f_{1s}(0)|\psi^f_{1s}(t)\rangle = \Sigma c_j^*(0)c_j(t)\exp(-itE'_j)$, respectively. If the time evolution scheme generates no errors, the coefficients $c_j(t)$ are time-independent, i.e., $c_j(t) = c_j(0)$. The time dependence of $c_j(t)$ originates from the inaccuracy of the time evolution scheme.

In this subsection, we use $\alpha=28.3$, $\beta=0.2$, and $\gamma=32$. Around these values, the results are insensitive to α, β, and γ. We test transformations by changing n and ν in Eq. (2.18a). As shown in Sec. II C, near $\xi=0$, the transformed wave function changes as $\approx\sqrt{(1+n\nu)\beta}\,\xi^{(2n\nu+1)/2}/\alpha^{n\nu}$. Since we apply the finite difference method, the transformed wave function must change linearly or quadratically with ξ: $n\nu$ must be $\frac{1}{2}$ or $\frac{3}{2}$. No further constraint on n or ν is found. In what follows, we numerically test two cases for $n\nu=\frac{1}{2}$ and the $n=1$ and $\nu=\frac{3}{2}$ case.

1. The n=1 and ν=½ transformation

Shown in Fig. 1 are norms and overlaps for the three-point finite difference scheme. The norms are denoted by bold lines and the absolute values of overlaps are denoted by thin lines. Two cases of different grid spacings are compared: Case (a) $\Delta\xi=0.26$ and $\Delta\zeta=0.26$ (lines with open circles); Case (b) $\Delta\xi=0.13$ and $\Delta\zeta=0.13$ (solid lines). The grid boundaries are chosen as $\xi_{\max}=65.0$ (the grid end in ρ is 54.3) and $\zeta_{\max}=55$ (the corresponding grid ends in z are ± 52.9). For Case (a), $N_\xi=250$ and $N_\zeta=423$. The time step used to evolve the wave function is $\Delta t=0.05$ throughout this paper. The initial wave function $\psi^f_{1s}(0)$ in the grid representation contains other states than ψ'_{1s}. As shown in Fig. 1, the interference between ψ'_{1s} and the main contaminant ψ'_{2s} induces an oscillation in the absolute value of the overlap.

The discretized ground state ψ'_{1s} is obtained by operating an energy filter on $\psi^f_{1s}(0)$ and eliminating the excited components.[42] The norm $\langle\psi'_{1s}(t)|\psi'_{1s}(t)\rangle$ and the overlap $|\langle\psi'_{1s}(0)|\psi'_{1s}(t)\rangle|$ do not change up to 6 or 7 digits. This proves that the coefficients $c_j(t)$ in Eq. (3.1) are nearly time-independent, i.e., $c_j(t)=c_j(0)$. The source of phase errors arising in the time evolution of the wave function is, therefore, only the inaccuracy of eigenvalues of the discretized Hamiltonian $\hat{H}'_0$. For the ground state of $\hat{H}'_0$, the virial theorem holds well; the ratio of the potential energy to the kinetic energy is -1.990 for Case (a) and -1.997 for Case (b).

Except $\alpha=0$ (or $n\nu=0$), the finite difference representation of Eq. (2.19) on the grid points $\xi_j = j\Delta\xi$ ($j=1$ to N_ξ) is not symmetric, as mentioned in Sec. II C.

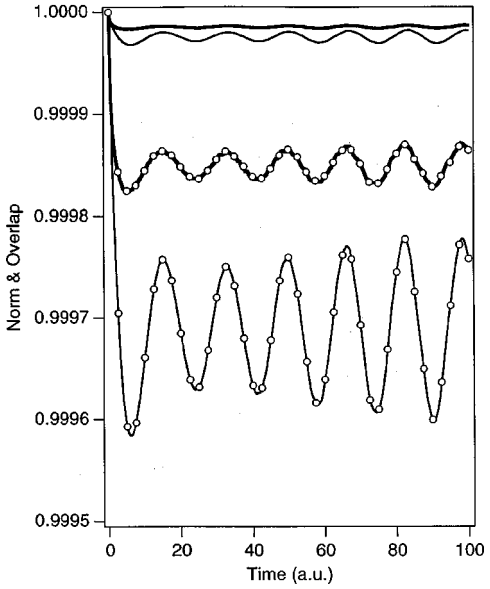

FIG. 1. Norms and overlaps of the $1s$ state calculated by the three-point finite difference scheme for $n=1$ and $\nu=\frac{1}{2}$. The norms are denoted by bold lines and the absolute values of overlaps are denoted by thin lines. The parameters for variable transformations are as follows: $\alpha=28.3$, $\beta=0.2$, and $\gamma=32$. Two cases of different grid spacings are compared: Case (a) $\Delta\xi=0.26$ and $\Delta\xi=0.26$ (lines with open circles); Case (b) $\Delta\xi=0.13$ and $\Delta\zeta=0.13$ (solid lines). The grid boundaries are chosen as $\zeta_{\max}=55$ (the corresponding grid ends in z are ± 52.9) and $\xi_{\max}=65.0$ (the grid end in ρ is 54.3). For Case (a), $N_\xi=250$ and $N_\zeta=423$. The time step used to evolve the wave function is $\Delta t=0.05$.

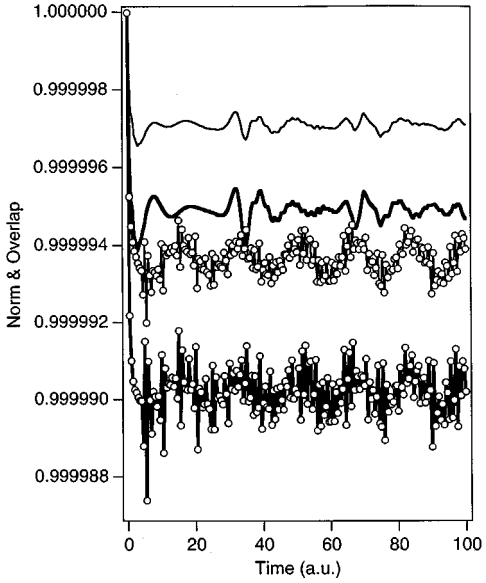

FIG. 2. $1s$ norms and overlaps calculated by the five-point finite difference scheme. The two Cases (a) and (b) are the same as in Fig. 1.

$$\langle j|K_\xi|j+1\rangle=-\frac{1}{2\mu\Delta\xi^2 f'^2(\xi_j)}\left[1-\frac{\Delta\xi f''(\xi_j)}{f'(\xi_j)}\right], \quad (3.2a)$$

$$\langle j+1|K_\xi|j\rangle=-\frac{1}{2\mu\Delta\xi^2 f'^2(\xi_{j+1})}\left[1+\frac{\Delta\xi f''(\xi_{j+1})}{f'(\xi_{j+1})}\right]. \quad (3.2b)$$

In what follows, we abbreviate matrix elements $\langle j|K_\xi|j'\rangle$ between points j and j' as $K_{j,j'}$. The ratio $K_{j+1,j}/K_{j,j+1}$ is about $\frac{5}{4}$ for $j=1$ (the next point to the $\xi=0$) and about 28/27 for $j=2$. However, except these few points near $\xi=0$, the asymmetry is negligible. As $\Delta\xi$ decreases, the leakage in norm decreases. The grid representation of Eq. (2.19) is hence virtually symmetric for typical values of grid spacings. For excited states such as ψ^f_{2s}, whether stationary or not, the leakage in norm is much smaller than that in the $1s$ case (at least by a factor of 1), which reflects the fact that the asymmetric part becomes negligible at large j. The simplest way to avoid the leakage in norm is to start from the ground state of the discretized Hamiltonian $\hat{H}'_0$.

While the three-point finite difference formulas for the first and second derivatives are accurate up to the orders of $\Delta\xi$, and $\Delta\zeta$, the five-point versions are accurate up to the orders of $\Delta\xi^3$ and $\Delta\zeta^3$. The norm and overlap for the five-point scheme are plotted in Fig. 2. The two cases (a) and (b) are the same as in Fig. 1. Comparing Figs. 1 and 2, one finds that the quality of the numerical scheme is drastically improved by the use of the five-point finite difference scheme. As shown in Fig. 2, $\sqrt{\langle\psi^f_{1s}(t)|\psi^f_{1s}(t)\rangle}\approx|\langle\psi^f_{1s}(0)|\psi^f_{1s}(t)\rangle|$. This means that $c_{1s}(t)\approx 1$ and $c_j(t)\approx 0$ for $j\neq 1s$. The generation of excited states of $\hat{H}'_0$ is negligible as well as the leakage in norm.

For the five-point representation, the eigenvalues of $\hat{H}'_0$ are highly accurate; the ground-state energy is $-0.499\,43$ for Case (a) and $-0.499\,71$ for Case (b). The virial theorem is also fulfilled to very high accuracy; for the ground state of $\hat{H}'_0$, the ratio of the potential energy to the kinetic energy is -1.9974 for Case (a) and -1.9998 for Case (b).

The solutions of the three- and five-point schemes converge to that of the Schrödinger equation by reducing $\Delta\xi$, $\Delta\zeta$, and Δt; that is, both schemes are consistent with the Schrödinger equation. For the parameters chosen in Figs. 1 and 2, the error does not grow exponentially with time. Practically, the method of the $n=1$ and $\nu=\frac{1}{2}$ transformation is unconditionally stable. For the cylindrical coordinate system, the accuracy is hardly improved by using higher order finite differences nor by using smaller spacings. For Case (a), the absolute value of the overlap is about 0.87 for the three-point scheme and is 0.88 for the five-point scheme; for Case (b) the values go up by 0.02 to 0.03.

2. The $n=1$ and $\nu=\frac{3}{2}$ transformation

Next we test the transformation of $n=1$ and $\nu=3/2$. A result for the five-point scheme is shown in Fig. 3. All the parameters are the same as used in Case (a). The norm is denoted by a dotted line and the overlap is denoted by a solid line. Since the relation $\sqrt{\langle\psi^f_{1s}(t)|\psi^f_{1s}(t)\rangle}\approx|\langle\psi^f_{1s}(0)|\psi^f_{1s}(t)\rangle|$ again holds, the rapid oscillations are attributed to the change in $c_{1s}(t)$. Comparing Case (a) in Fig. 2, one finds that the accuracy is a little worse for the present transformation than for the $n=1$ and $\nu=\frac{1}{2}$ transformation. While the $1s$ transformed wave function for $n\nu=\frac{1}{2}$ increases linearly with ξ around the nucleus, it increases quadratically for $n\nu=\frac{3}{2}$. For both cases, the initial norm at $t=0$ is accurate up to 7 or 8 digits. The difference in accuracy

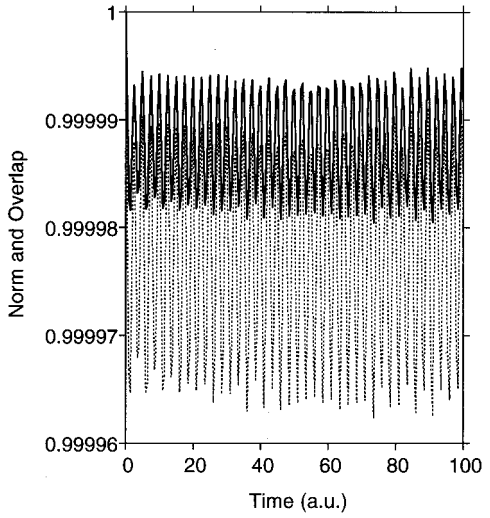

FIG. 3. 1*s* norm and overlap calculated by the five-point finite difference scheme for $n=1$ and $\nu=\frac{3}{2}$. All the parameters are the same as used in Case (a). The norm is denoted by a dotted line and the overlap is denoted by a solid line.

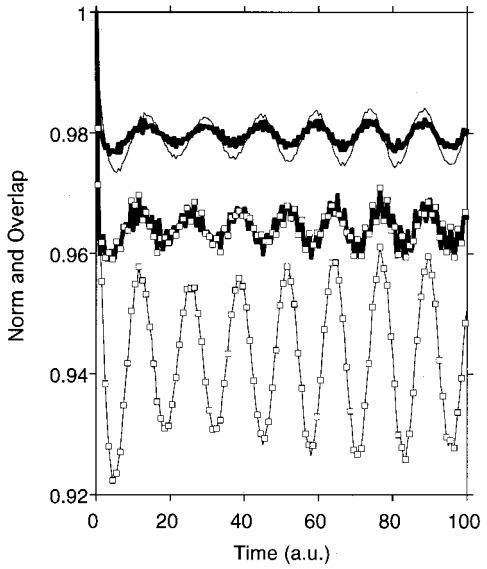

FIG. 4. Comparison between two transformations of $n\nu=\frac{1}{2}$. The grid spacings used here are much larger than in Case (a): $N_\xi=63$ and $N_\xi=107$ (the other parameters are the same as before). The bold and thin lines, without marks, denote the norm and overlap for the $n=\frac{1}{2}$ and $\nu=1$, respectively; the bold and thin lines, with open squares, denote the norm and overlap for the $n=1$ and $\nu=\frac{1}{2}$.

comes from the fact that the asymmetry of the finite difference representation of Eq. (2.19) on grid points $\xi_j=j\Delta\xi$ is severer for the present transformation than for the $n=1$ and $\nu=\frac{1}{2}$ transformation. Using Eq. (3.1), we can compare the two cases for the three-point scheme. For the present transformation, the ratio $K_{j+1,j}/K_{j,j+1}$ is about $-\frac{7}{16}$ for $j=1$ and about $(\frac{4}{3})^2$ for $j=2$. The deviation of $K_{j+1,j}/K_{j,j+1}$ from unity is large in comparison with the $n=1$ and $\nu=\frac{1}{2}$ case. This is due to the fact that $f(\xi)$ changes steeper for the present transformation than the $n=1$ and $\nu=\frac{1}{2}$ transformation.

3. The $n=\frac{1}{2}$ and $\nu=1$ transformation

Among those we have tested, the $n=1$ and $\nu=1/2$ transformation provides most accurate results when $\Delta\xi$ is as small as in Case (a). For low bound states, the accuracy is improved by increasing α. Extremely large α, however, should not be used when higher excited/continuum states are involved in the dynamics of the wave packet because the grid spacing in ρ space increases as $\Delta\rho\propto f'\approx(1+n\nu)(\xi/\alpha)^{n\nu}$ until ξ reaches α. In the range where the potential is nearly flat, the grid spacing $\Delta\rho$ must be constant. For Eq. (2.18a), f' becomes constant where $\xi>\alpha$. Different transformations of Eq. (2.18a) should be compared for a fixed α.

When computational ability is limited or large grids are required to propagate the wave packet, we recommend to use another transformation of $n\nu=\frac{1}{2}$, i.e., the $n=\frac{1}{2}$ and $\nu=1$ case. This transformation is compared in Fig. 4 with the $n=1$ and $\nu=\frac{1}{2}$ case. The same $\alpha=28.3$ is used. The grid spacings used here are much larger than in Case (a): $N_\xi=63$ and $N_\xi=107$ (the other parameters are the same as before). The bold and thin lines without marks denote the norm and overlap for the $n=\frac{1}{2}$ and $\nu=1$, respectively; the bold and thin lines with open squares denote the norm and overlap for the $n=1$ and $\nu=\frac{1}{2}$. For the present grid points, as shown in Fig. 4, the $n=\frac{1}{2}$ and $\nu=1$ transformation is superior to the $n=1$ and $\nu=\frac{1}{2}$ one. The reason is as follows. For large spacings, while the accuracy of the finite difference method in evaluating the differentials is nearly the same for both transformations, the asymmetry in the grid representation of K_ξ near $\xi=0$ is much smaller for the $n=\frac{1}{2}$ and $\nu=1$ transformation than for the $n=1$ and $\nu=\frac{1}{2}$ one. When the spacings are as small as in Case (a), while the asymmetry is the same for both transformations, the accuracy of the finite difference method is higher for the $n=1$ and $\nu=\frac{1}{2}$ transformation than for the $n=\frac{1}{2}$ and $\nu=1$ one.

B. Phase space analysis in terms of a quasi-potential

As shown in this paper, variable transformation together with the consistent transformation of the wave function is indispensable for the wave packet dynamics in Coulomb systems. In the following, using the phase space analysis,[48] we examine why the efficiency of the grid representation is enhanced by the variable transformations tested in Sec. III A. In general, wave packets decay exponentially in classically forbidden regions of phase space. The representation efficiency can therefore be optimized by minimizing the missing phase space, i.e., the classically allowed phase space that cannot be covered by the grid representation or by minimizing the wasted phase space area relative to the phase space covered by the grid representation (Fattal *et al.*[48] have applied the method to the H_2^+ eigenvalue problem). The maximum momentum with ξ in the grid representation is given by $P_{\xi,\max}=\pi/\Delta\xi$. The function $f(\xi)$ should be chosen so that the phase space between $-P_{\xi,\max}$ and $P_{\xi,\max}$ covers the classically allowed phase space as well as possible.

The definition of the classically forbidden region for the transformed Hamiltonian (2.11), $\hat{H}$ is, however, rather arbi-

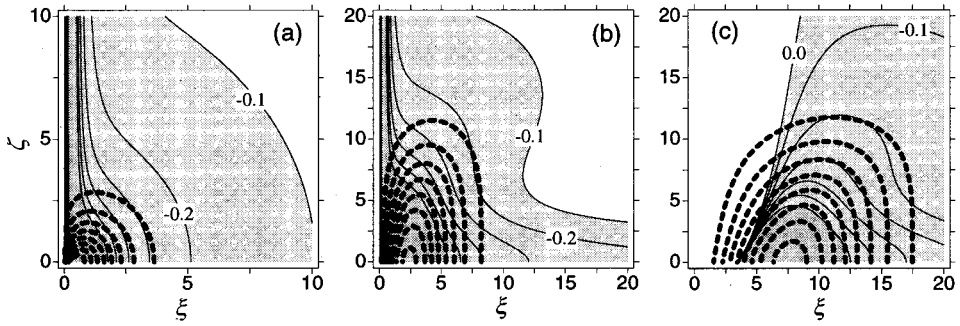

FIG. 5. Quasi-potentials and $1s$ transformed wave functions: (a) Cylindrical coordinates $\alpha=0$ and $\beta=1$; (b) $\nu=\frac{1}{2}$ and $n=1$; (c) $\nu=\frac{3}{2}$ and $n=1$. For (b) and (c), the following parameters are used as before: $\alpha=28.3$, $\beta=0.2$, and $\gamma=32$. The quasi-potentials are drawn by thin contour lines. The energy intervals between thin lines are 0.1. The energies in the black-painted region along $\xi=0$, which appears in (a) and (b), are below -5. The $1s$ transformed wave functions for the three cases are drawn by bold broken contour lines.

trary. To define it, we must interpret $\hat{H}$ as a classical Hamiltonian. We first recast $\hat{H}$ into

$$\hat{H}=K_R+T_\xi+T_\zeta+V_{\text{quasi}}, \tag{3.3}$$

where

$$V_{\text{quasi}}(\xi,\zeta)=\frac{1}{4\mu f'^4(\xi)}\left[\frac{7}{2}f''^2(\xi)-f'(\xi)f'''(\xi)\right]-\frac{1}{8\mu f^2(\xi)}+\frac{1}{4\mu g'^4(\zeta)}\left[\frac{7}{2}g''^2(\zeta)-g'(\zeta)g'''(\zeta)\right]+\frac{m^2}{2\rho^2}+V+V_{\mathcal{E}}. \tag{3.4}$$

We then interpret the operators in $\hat{H}$ as follows. The Hermitian operators T_ξ and T_ζ with ''effective masses'' $\mu f'^2(\xi)$ and $\mu g'^2(\zeta)$ can be regarded as the kinetic energies for the ξ and ζ degrees of freedom in the transformed representation. Then, V_{quasi} is regarded as the ''quasi-potential.''

Quasi-potentials for the hydrogen atom case are shown in Fig. 5 by thin contour lines: (a) Cylindrical coordinates ($\alpha=0$ and $\beta=1$); (b) $n=1$ and $\nu=\frac{1}{2}$; (c) $n=1$ and $\nu=\frac{3}{2}$. For (b) and (c), the following parameters are used as before: $\alpha=28.3$, $\beta=0.2$, and $\gamma=32$. For the cylindrical coordinate system

$$V_{\text{quasi}}(\xi,\zeta=0)=-1/\xi-1/8\mu\xi^2. \tag{3.5a}$$

For the generalized cylindrical coordinate system, the quasi-potential takes

$$V_{\text{quasi}}(\xi,\zeta=0)\approx-\frac{\alpha^{n\nu}}{\xi^{1+n\nu}}+\frac{\alpha^{2n\nu}(2n\nu+1)(2n\nu-1)}{8\mu\xi^{2(n\nu+1)}(n\nu+1)^2}, \tag{3.5b}$$

in the region where $\xi\ll\alpha$. When the cylindrical coordinate system or the $n\nu=\frac{1}{2}$ transformations are employed, V_{quasi} is negative infinity at $\xi=\zeta=0$; for the $n\nu=\frac{3}{2}$ transformation, V_{quasi} is *positive* infinity at the origin $\xi=\zeta=0$.

An eigenfunction of $\hat{H}$ is the transformed representation of the corresponding eigenfunction of H. The $1s$ transformed wave functions for the three cases are drawn in Fig. 5 by bold broken contour lines. As the case goes from (a) to (c), the peak of the $1s$ transformed wave function is more distant from the nucleus relative to the whole shape. The spatial diffuseness of the transformed wave function in case (b) or (c) is due to its lighter effective masses near the origin. The success of the $n\nu=\frac{1}{2}$ transformation can be attributed to the fact that the transformed wave function increases to the peak more slowly than that for the cylindrical coordinate system.

Although the $n\nu=\frac{3}{2}$ transformation is not the best one as long as the ADI is employed, it has an interesting feature: The quasi-potential is repulsive near the origin. As shown in Fig. 5(c), the potential minimum exists off the origin (at $\xi\approx5$ and $\zeta=0$); the peak of the $1s$ transformed wave function is located near the potential minimum. The amplitude penetrates the repulsive potential because the effective mass $\mu f'^2(\xi)$ becomes smaller with decreasing ξ.

Here we replace the differential operators in T_ξ and T_ζ with classical momenta P_ξ and P_ζ as $P_\xi^2=-\partial^2/\partial\xi^2$ and $P_\zeta^2=-\partial^2/\partial\zeta^2$. To observe the representation efficiency in the 4D phase space, different cuts are required. The 2D (ξ,P_ξ) cut is taken for the worst case where $\zeta=0$ and $P_\zeta=0$. Contour maps of $P_\xi^2/2\mu f'^2+V_{\text{quasi}}(\xi,\zeta=0)$ are presented in Fig. 6. The energies in the shaded areas are below the $1s$ energy -0.5.

For the cylindrical coordinate system, as shown in Fig. 6(a), the shaded area above a given maximum momentum $P_{\xi,\max}(=\pi/\Delta\xi)$ decreases slowly with increasing $P_{\xi,\max}$: The high momentum part cannot be fully covered by any grid spacing. On the other hand, in Fig. 6(b), the shaded area above $P_{\xi,\max}$ decreases faster with increasing $P_{\xi,\max}$. To discuss the representation efficiency quantitatively, we define the missing volume in phase space as

$$V_{\text{miss}}=2\int_{\pi/\Delta\xi}^{\infty}\xi dP_\xi, \tag{3.6}$$

where P_ξ is the required momentum for energy E given as a function of ξ as

$$P_\xi=f'(\xi)\{2\mu[E-V_{\text{quasi}}(\xi,\zeta=0)]\}^{1/2}. \tag{3.7}$$

For the cylindrical coordinate system, one finds from Eqs. (3.5a) and (3.7) that near $\xi=0$ the required momentum increases with decreasing ξ as

$$P_\xi = \xi^{-1}/2. \tag{3.8}$$

For $n\nu = \frac{1}{2}$, in the range where $\xi \ll \alpha$, we have

$$P_\xi = 3\sqrt{\mu/2\alpha^{1/2}}\,\xi^{-1/4}. \tag{3.9}$$

For Eqs. (3.8) and (3.9), we obtain

$$V_{\text{miss}} = \infty (\text{logarithmic divergence})$$
$$\text{for the cylindrical coordinate system,} \tag{3.10a}$$

$$\approx \frac{27\mu^2}{2\alpha}\left(\frac{\Delta\xi}{\pi}\right)^3 \quad \text{for } n\nu = \tfrac{1}{2}. \tag{3.10b}$$

The $n\nu = \frac{1}{2}$ transformations are validated by the fact that the missing volume decreases with decreasing $\Delta\xi$.

For $n\nu = 3/2$, $V_{\text{quasi}}(\xi, \zeta = 0) = 4\alpha^3/25\mu\xi^5$ near $\xi = 0$. The momentum required does not diverges at $\xi = \zeta = 0$. Even with finite sized of $\Delta\xi$, the whole area of the classically allowed phase space can be efficiently covered by a rectangle with sides of $[0, \xi_{\max}]$ and $[0, \pi/\Delta\xi]$. Although the present finite difference schemes do not fully take this advantage as mentioned in Sec. III A, the development of efficient numerical schemes utilizing the $n\nu = \frac{3}{2}$ transformation remains as a future possibility.

The quality of the form of $g(\zeta)$ in Eq. (2.18b) is the same as the function proposed by Fattal *et al.*[48]

$$r = Q - a \arctan(bQ), \tag{3.11}$$

where r is the unscaled coordinate and Q is the scaled coordinate. For $Q \ll b^{-1}$, $dr/dQ = 1 - ab$; for $Q \gg b^{-1}$, $dr/dQ = 1$.

C. 3D packet simulation of H_2^+

The two transformations of $n\nu = \frac{1}{2}$ are also tested for the 3D H_2^+. The dissociative process is taken as the example. To that end, first, the exact ground state (of the vibrational quantum number $v = 0$ in $1\sigma_g$) of the 3D full system is prepared by operating an energy filter on an approximate ground state to eliminate the excited components.[42] Next, the molecule is excited by a weak ultrashort pump pulse from the ground state onto $1\sigma_u$. The pump field is assumed as

$$\mathcal{E}(t) = \sin\frac{\pi(t+T)}{T}\sin\omega(t+T)$$
$$\text{for } -T \leqslant t \leqslant 0, \quad \text{otherwise } \mathcal{E}(t) = 0, \tag{3.12}$$

where T is the pulse duration. The frequency used is $\omega = 0.43$ (105 nm) which corresponds to the energy gap between $1\sigma_g$ and $1\sigma_u$ at the equilibrium internuclear distance $R = 2.0$ and the pulse duration is $T = 100$ (2.5 fs). The pump field is put into the dipole interaction Eq. (2.4). A perturbative iteration scheme[59] with respect to the dipole interaction is used to simulate the excitation process of the 3D packet in the weak field limit. To perform the time evolution of the packet required in the scheme, we solve the transformed Schrödinger Eq. (2.10) by using the ADI method. At the end of the pump process ($t = 0$), the electronically excited component of the packet (the first-order component with respect to the dipole interaction) is normalized to unity. After $t = 0$, the dissociative motion is pursued; the excited component is propagated without an external field.

To illustrate the packet dynamics, we integrate the 3D packet over ρ. Snapshots of the probability $\int |\phi(R, \rho, z)|^2 \rho d\rho$ are shown in Fig. 7. The grid ends are chosen as $\rho_{\max} = 8.83$ and $z_{\max} = 10$. We choose $\alpha = 28.3$ and $\Delta R = 0.05$. In Fig. 7(a), $n = 1$ and $\nu = \frac{1}{2}$. The numbers of grid points are enough large, although no transformation is used for z coordinate; $N_\xi = 151$ and $N_\zeta = 207$ ($\Delta\xi = 0.1$, $\Delta\zeta = 0.1$). The excitation and dissociation dynamics in Fig. 7(a) is regarded as the exact one. As known from the existence of the nodal line at $z = 0$, the packet prepared by the pump pulse is electronically $1\sigma_u$. The errors in electronic phases attached to the wave function are small enough to simulate the excitation process; the vibrational phases are also accurate enough to simulate dissociation process. In Fig. 7(b), the $n = \frac{1}{2}$ and $\nu = 1$ transformation is used. The numbers of grid points are reduced to $N_\xi = 19$ and $N_\zeta = 57$. The main features of the dynamics are well simulated even with the parameter set used in Fig. 7(b), except that the wave packet trails the skirt of low density and the relative nuclear velocity is a little larger than the exact one.

IV. SUMMARY AND CONCLUSIONS

We established the dual transformation technique for wave packet dynamics. The technique contains both the vari-

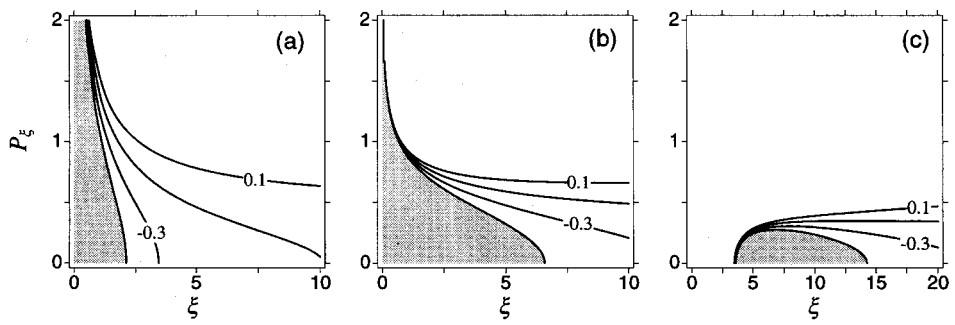

FIG. 6. Contour maps of $P_\xi^2/2\mu f'^2 + V_{\text{quasi}}(\xi, \zeta = 0)$ in the 2D (ξ, P_ξ) phase space for $\zeta = 0$ and $P_\zeta = 0$. The energy intervals are 0.2 and the energies in the shaded areas are below the $1s$ energy -0.5. The notations and parameters for (a), (b), and (c) are the same as in Fig. 5.

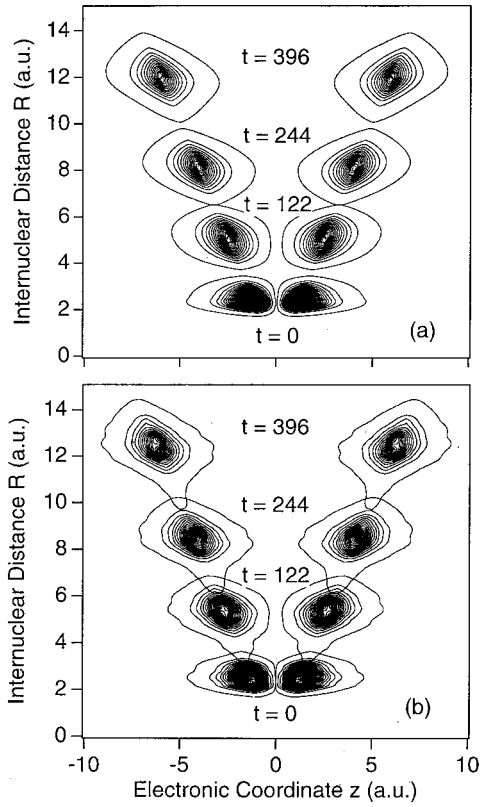

FIG. 7. Contour maps of the time-dependent probability $\int|\phi(\rho,z,R)|^2\rho d\rho$ obtained by integrating the 3D packet with respect to ρ. A sequence of snapshots shows that the packet pumped on $1\sigma_u$ moves toward larger internuclear distance. The origin $t=0$ in time is the end of the pump pulse. The grid ends are chosen as $\rho_{\max}=8.83$ and $z_{\max}=10$. In Fig. 7(a), $n=1$ and $\nu=\frac{1}{2}$. The numbers of grid points are large enough; $N_\xi=151$ and $N_\zeta=207$ ($\Delta R=0.05$). In Fig. 7(b), the $n=1$ and $\nu=\frac{1}{2}$ transformation is used. The numbers of grid points are reduced to $N_\xi=19$ and $N_\zeta=57$ ($\Delta R=0.05$).

able transformation of the Hamiltonian and the transformation of the wave function with a normalization constraint. We applied it to Coulomb systems, i.e., the H atom and the 3D model of H_2^+. The cylindrical coordinates are transformed as $\rho=f(\xi)$ and $z=g(\zeta)$, where ξ and ζ are scaled cylindrical coordinates. The functions f and g must possess the following features under the normalization constraint Eq. (2.8): The transformed wave function is zero and analytic at the nuclei; the equal spacings in the new coordinates correspond to grid spacings in the cylindrical coordinates that are small near the nuclei and are large at larger distances therefrom. The time evolution is carried out by the ADI. The operation of the Hamiltonian on the wave function, which is required in the ADI scheme, is implemented by using finite difference formulas.

In existing methods, the shape of the Coulomb potential has been frequently modified by a variety of means. An example is the softened Coulombic form $-(r^2+\delta^2)^{-1/2}$ with an ambiguous softening parameter δ which eliminates the singularity at the nucleus $r=0$.[60] Another example is to spread the positive nuclear charge uniformly over an area equal to about one grid spacing.[14,33] This introduces an additional potential at the $r=0$ boundary. The radius can be varied so that the ground-state wave function obtained satisfies the virial theorem. As mentioned in Sec. III A, when the variable transformation functions and the grid spacings are properly chosen in the dual transformation, the virial theorem is fulfilled to very high accuracy. For the dual transformation, the singularity is removed without violating the Schrödinger equation and any variational procedure is unnecessary.

The explicit form Eq. (2.18a) for $f(\xi)$ proposed in this paper has three parameters α, n, and ν. We have tested transformations of different n and ν for the time evolution of a field-free H atom in the $1s$ state; the norm and overlap of the $1s$ state calculated by our method are compared with exact ones. The $n=1$ and $\nu=\frac{1}{2}$ transformation provides most accurate results when $\Delta\xi$ is as small as in Case (a) in Sec. III. For large spacings, the $n=\frac{1}{2}$ and $\nu=1$ transformation is superior to the $n=1$ and $\nu=\frac{1}{2}$ one. We have also applied the two transformations of $n\nu=\frac{1}{2}$ to the dissociation dynamics in the 3D model of H_2^+. For the $n=\frac{1}{2}$ and $\nu=1$ transformation, the main features of the dynamics are well simulated even with moderate numbers of grid points. Larger systems such as H_2 should be handled by using the $n=\frac{1}{2}$ and $\nu=1$ transformation.

The transformed Hamiltonian is divided into a kinetic energy and a potential; the phase space covered by the grid representation is estimated. The validity of the $n\nu=\frac{1}{2}$ transformations is also enforced by the fact that the missing volume in phase space decreases with decreasing $\Delta\xi$. On the other hand, for the cylindrical coordinate system, the missing volume is infinity. We have also tested the transformation of $n=1$ and $\nu=\frac{3}{2}$. Although the accuracy in the $n=1$ and $\nu=\frac{3}{2}$ case is a little worse than in the $n=1$ and $\nu=\frac{1}{2}$ case, all the phase space can be fully covered by $n\nu=\frac{3}{2}$ transformations even for finite sizes of $\Delta\xi$ and $\Delta\zeta$. This advantage of $n\nu=\frac{3}{2}$ transformations may be utilized in future studies.

In this paper, the wave functions are expanded in cylindrical coordinates. Another choice is to use spherical coordinates r, θ, and φ. The wave function can be expanded in spherical harmonics as[14,33,61]

$$\sum_l \phi_l(r)Y_{lm}(\theta,\varphi).$$

The dual transformation technique is in principle applicable to any coordinate systems. For a variable transformation $r=h(\eta)$, the original radial wave functions $\{\phi_l(r)\}$ need to be converted as

$$\psi_l(\eta)=h(\eta)\sqrt{h'(\eta)}\,\phi_l(h(\eta)).$$

Then, one can obtain the coupled equations for the transformed wave functions $\{\psi_l(\eta)\}$. If the field-free potential $V(r,\theta,\varphi)$ is spherically symmetric as in hydrogenlike atoms (this is not the case for H_2^+), the time propagation for $\{\psi_l(\eta)\}$ in the presence of a linearly polarized field can be efficiently carried out using the Peaceman–Rachford method.[33] The function $h(\eta)$ should be chosen so that the transformed wave functions satisfy the three requirements in the dual transformation. Generally speaking, the procedure in solving a given problem is to choose the best coordinate system for describing the dynamics and then to apply the dual transformation.

In conclusion, the dual transformation is a solid technique that provides efficient time evolution schemes for Coulomb systems. The accuracy and stability reach the level usually required for wave packet dynamics.

ACKNOWLEDGMENTS

This work was supported in part by the Department of High-Density Optical Pulse Generation and Advanced Material Control Techniques. We would like to express our appreciation to Professor Y. Fujimura and Professor J. Manz for valuable discussion.

[1] I. Kawata, H. Kono, and Y. Fujimura, Chem. Phys. Lett. **289**, 546 (1998).
[2] I. Kawata, H. Kono, and Y. Fujimura, J. Chem. Phys. **110**, 11152 (1999).
[3] M. Grønager and N. E. Henriksen, J. Phys. Chem. A **102**, 4277 (1998).
[4] L. V. Keldysh, Sov. Phys. JETP **20**, 1307 (1965).
[5] F. H. M. Faisal, J. Phys. B **6**, L89 (1973).
[6] H. R. Reiss, Phys. Rev. A **22**, 1786 (1980).
[7] S. Augst, D. D. Meyerhofer, D. Strickland, and S. L. Chin, J. Opt. Soc. Am. B **8**, 858 (1991).
[8] M. V. Ammosov, N. B. Delone, and V. P. Krainov, Sov. Phys. JETP **64**, 1191 (1986).
[9] P. B. Corkum, Phys. Rev. Lett. **71**, 1994 (1993).
[10] J. H. Eberly, J. Javanainen, and K. Rzazewski, Phys. Rep. **204**, 331 (1991).
[11] P. B. Corkum, N. H. Burnett, and F. Brunel, Phys. Rev. Lett. **62**, 1259 (1989).
[12] M. Lewenstein, K. C. Kulander, K. J. Schafer, and P. H. Bucksbaum, Phys. Rev. A **51**, 1495 (1995).
[13] K. Burnett, V. C. Reed, J. Cooper, and P. L. Knight, Phys. Rev. A **45**, 3347 (1992).
[14] J. L. Krause, K. J. Schafer, and K. C. Kulander, Phys. Rev. A **45**, 4998 (1992).
[15] K. J. Schafer and K. C. Kulander, Phys. Rev. A **45**, 8026 (1992).
[16] T. Zuo, A. D. Bandrauk, M. Ivanov, and P. B. Corkum, Phys. Rev. A **51**, 3991 (1995).
[17] P. Moreno, L. Plaja, V. Malyshev, and L. Roso, Phys. Rev. A **51**, 4746 (1995).
[18] I. Zhou, J. Peatross, M. M. Murnane, and H. C. Kapteyn, Phys. Rev. Lett. **76**, 752 (1996).
[19] I. P. Christov, J. Zhou, J. Peatross, A. Rundquist, M. M. Murnane, and H. C. Kapteyn, Phys. Rev. Lett. **77**, 1743 (1996).
[20] C. Cornaggia, J. Lavancier, D. Normand, J. Morellec, P. Agostini, J. P. Chambaret, and A. Antnetti, Phys. Rev. A **44**, 4499 (1991).
[21] C. Cornaggia, D. Normand, and J. Morellec, J. Phys. B **25**, L415 (1992).
[22] L. J. Fransinski, P. A. Hatherly, K. Codling, M. Larsson, A. Persson, and C.-G. Wahlstrom, J. Phys. B **27**, L109 (1994).
[23] P. A. Hatherly, M. Stankiewicz, K. Codling, L. J. Frasinski, and G. M. Cross, J. Phys. B **27**, 2993 (1994).
[24] S. Chelkowski and A. D. Bandrauk, J. Phys. B **28**, L723 (1995).
[25] T. Zuo and A. D. Bandrauk, Phys. Rev. A **52**, R2511 (1995).
[26] T. D. G. Walsh, F. A. Ilkov, S. L. Chin, F. Châteauneuf, T. T. Nguen-Dang, S. Chelkowski, A. D. Bandrauk, and O. Atabek, Phys. Rev. A **58**, 3922 (1998).
[27] A. D. Bandrauk, Comments Atomic Molecular Phys. (in press).
[28] T. Seideman, M. Yu. Ivanov, and P. B. Corkum, Phys. Rev. Lett. **75**, 2819 (1995); M. Ivanov, T. Seideman, and P. Corkum, Phys. Rev. A **54**, 1541 (1996).
[29] D. M. Villeneuve, M. Yu. Ivanov, and P. B. Corkum, Phys. Rev. A **54**, 736 (1996).
[30] Ue-Li Pen and T. F. Jiamg, Phys. Rev. A **53**, 623 (1996).
[31] M. Horbatsch, J. Chem. Phys. **79**, 4382 (1983).
[32] M. Horbatsch, Phys. Rev. A **44**, R5346 (1991).
[33] K. C. Kulander, K. J. Schafer, and J. L. Krause, Adv. At. Mol. Phys. Suppl. **1**, 247 (1992).
[34] H. Yu, A. D. Bandrauk, and V. Sonnard, J. Math. Chem. **15**, 273 (1994).
[35] S. Chelkowski, T. Zuo, O. Atabek, and A. D. Bandrauk, Phys. Rev. A **52**, 2977 (1995).
[36] S. Chelkowski, C. Foisy, and A. D. Bandrauk, Phys. Rev. A **57**, 1176 (1995).
[37] Th. Mercouris, Y. Komninos, S. Dionissopoulou, and C. A. Nicolaides, Phys. Rev. A **50**, 4109 (1994).
[38] S. Dionissopoulou, Th. Mercouris, A. Lyras, Y. Komninos, and C. A. Nicolaides, Phys. Rev. A **51**, 3104 (1995).
[39] S. Dionissopoulou, Th. Mercouris, A. Lyras, and C. A. Nicolaides, Phys. Rev. A **55**, 4397 (1997).
[40] R. Kosloff, J. Phys. Chem. **92**, 2087 (1988).
[41] N. Balakrishnan, C. Kalyanaraman, and N. Sathyamurthy, Phys. Rep. **280**, 79 (1997).
[42] M. D. Feit, J. A. Fleck, Jr., and A. Steiger, J. Comput. Phys. **47**, 412 (1982); M. D. Feit and J. A. Fleck, Jr., J. Chem. Phys. **78**, 301 (1983).
[43] H. Kono and S. H. Lin, J. Phys. Chem. **84**, 1071 (1986).
[44] H. Kono, A. Kita, Y. Ohtsuki, and Y. Fujimura, J. Comput. Phys. **130**, 148 (1997).
[45] W. H. Press, S. A. Teukolsky, W. T. Vetterling, and B. P. Flannery, *Numerical Recipes* in FORTRAN, 2nd ed. (Cambridge, New York, 1992), Chap. 19.
[46] A. R. Mitchell, *Computational Methods in Partial Differential Equations* (Wiley, New York, 1969).
[47] N. N. Yanenko, *The Method of Fractional Steps* (Springer, New York, 1971).
[48] E. Fattal, R. Baer, R. Kosloff, and D. Kosloff, Phys. Rev. E **53**, 1217 (1996).
[49] J. R. Hiskes, Phys. Rev. **122**, 1207 (1961).
[50] C. Froese Fischer, *The Hartree–Fock Method for Atoms* (Wiley, New York, 1976), p. 223.
[51] E. Trefftz, A. Schlüter, K.-H. Dettmar, and K. Jörgens, Z. Astrophys. **44**, 1 (1957).
[52] L. V. Chernysheva, N. A. Cherepkov, and V. Radojevíc, Comput. Phys. Commun. **11**, 57 (1976).
[53] D. Heinemann, B. Fricke, and D. Kolb, Phys. Rev. A **38**, 4994 (1988).
[54] L. Laaksonen, D. Sundholm, and P. Pyykkö, Comput. Phys. Rep. **4**, 313 (1986).
[55] A. D. Becke, J. Chem. Phys. **76**, 6037 (1982).
[56] F. Gygi and G. Galli, Phys. Rev. B **52**, R2229 (1995); F. Gygi, *ibid.* **51**, 11190 (1995).
[57] R. Varga, *Matrix Iterative Analysis* (Prentice-Hall, Englewood Cliffs, 1962), p. 273.
[58] D. M. Yang and R. T. Gregory, *A Survey of Numerical Mathematics, Vol. II* (Reading, Addison-Wesley, 1973), p. 1097.
[59] H. Kono and Y. Fujimura, Chem. Phys. Lett. **184**, 497 (1991).
[60] J. Javanainen, J. Eberly, and Q. Su, Phys. Rev. A **38**, 3430 (1988).
[61] M. R. Hermann and J. A. Fleck, Jr., Phys. Rev. A **38**, 6000 (1988).